Development of a simple process to obtain luminescent $YVO_4:Eu^{3+}$ nanoparticles for Fiber Optic Dosimetry

Luciana Mentasti, Nahuel Martínez, Ileana A. Zucchi, Martín Santiago, Gastón Barreto

PII: S0925-8388(20)30991-9

DOI: https://doi.org/10.1016/j.jallcom.2020.154628

Reference: JALCOM 154628

To appear in: *Journal of Alloys and Compounds*

Received Date: 20 December 2019

Revised Date: 27 February 2020

Accepted Date: 2 March 2020

Please cite this article as: L. Mentasti, N. Martínez, I.A. Zucchi, Martí. Santiago, Gastó. Barreto, Development of a simple process to obtain luminescent $YVO_4:Eu^{3+}$ nanoparticles for Fiber Optic Dosimetry, *Journal of Alloys and Compounds* (2020), doi: https://doi.org/10.1016/j.jallcom.2020.154628.

Credit Author Statement

Development of a simple process to obtain luminescent $YVO_4:Eu^{3+}$ nanoparticles for Fiber Optic Dosimetry

Luciana Mentasti: methodology, investigation, writing- original draft.

Nahuel Martínez: methodology, investigation.

Ileana A. Zucchi: writing- review and editing, supervision.

Martín Santiago: writing- review and editing, conceptualization, supervision, funding acquisition.

Gastón Barreto: methodology, writing- original draft, funding acquisition, project administration.

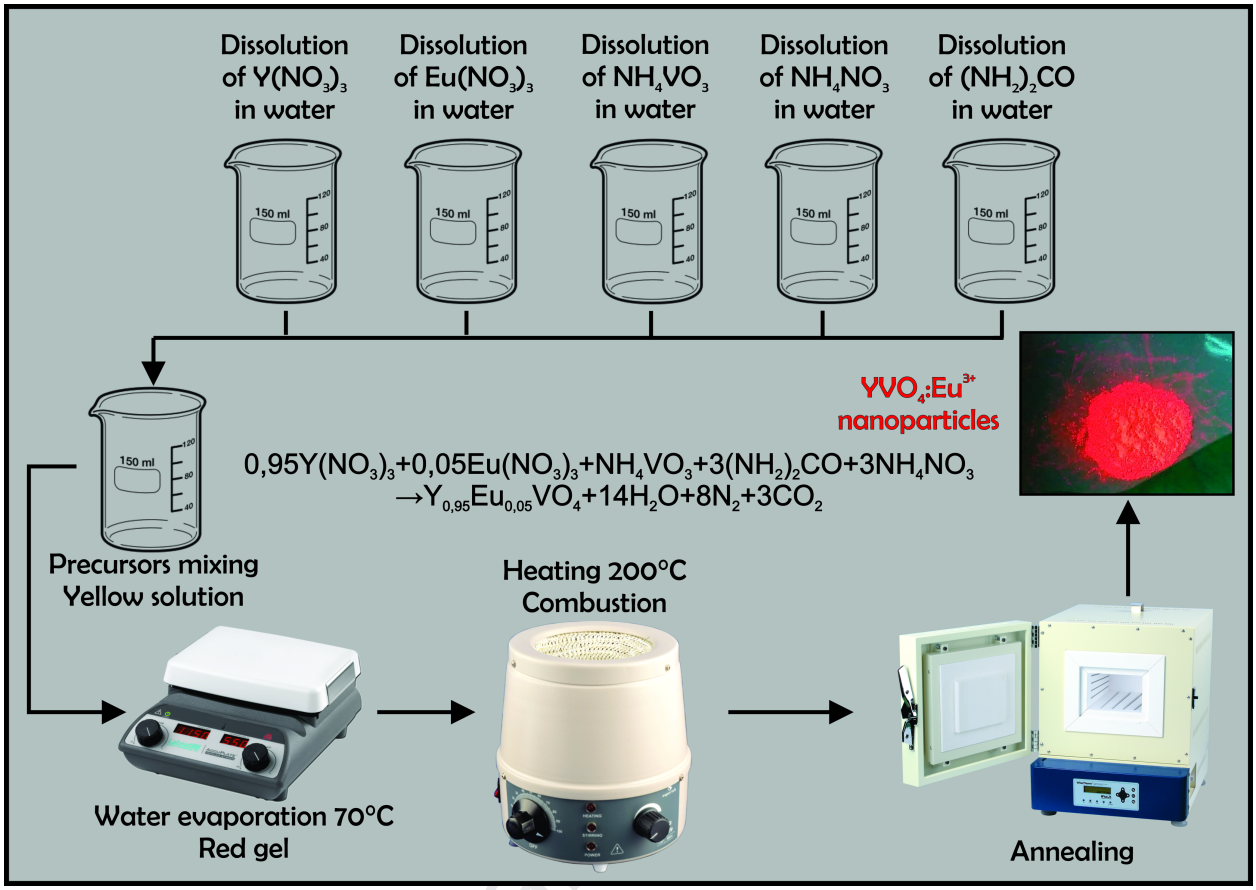
Dissolution of $Y(NO_3)_3$ in water
Dissolution of $Eu(NO_3)_3$ in water
Dissolution of NH_4VO_3 in water
Dissolution of NH_4NO_3 in water
Dissolution of $(NH_2)_2CO$ in water
150 ml
$YVO_4:Eu^{3+}$ nanoparticles
$0,95Y(NO_3)_3+0,05Eu(NO_3)_3+NH_4VO_3+3(NH_2)_2CO+3NH_4NO_3$
$\rightarrow Y_{0,95}Eu_{0,05}VO_4+14H_2O+8N_2+3CO_2$
Precursors mixing
Yellow solution
Heating 200°C
Combustion
Water evaporation 70°C
Red gel
Annealing

Development of a simple process to obtain luminescent $YVO_4:Eu^{3+}$ nanoparticles for Fiber Optic Dosimetry

Luciana Mentasti[a], Nahuel Martínez[a], Ileana A. Zucchi[b], Martín Santiago[a] and Gastón Barreto[a]*

[a] Center for Research in Physics and Engineering of the Center of Buenos Aires Province, CIFICEN (UNCPBA-CONICET-CICPBA). Pinto 399, B7400JWI, Olavarría, Buenos Aires, Argentina.

[b] Institute of Materials Science and Technology, INTEMA (UNMDP-CONICET), J. B. Justo 4302, 7600 Mar del Plata, Argentina

*Corresponding author, mail: gbarreto@fio.unicen.edu.ar. Av. del Valle 5737, Olavarría (CP7400), Buenos Aires, Argentina.

Abstract

$YVO_4:Eu^{3+}$ is a red emitter phosphor commercially available as micrometric powder due to its high luminescence efficiency under electron-beam excitation. Although some published results have demonstrated the potential of using this micrometer material in Fiber Optic Dosimetry systems, there is no information regarding its use on a nanometric scale. In order to obtain a nanometric material with high luminescent efficiency, a simple synthetic combustion method was developed and the results were compared with both, those of a commercial material and those obtained by a typical coprecipitation synthesis. A single crystalline phase was obtained when the combustion route was employed for the preparation meanwhile two crystalline phases were obtained via coprecipitation synthesis. The particle size of $YVO_4:Eu^{3+}$ obtained by combustion route ranges from 55 up to 200 nm. Fourier Transform Infrared Spectroscopy and Thermogravimetric Analysis indicated that annealing at 600°C promote the degradation of the impurities that remained adsorbed onto nanoparticles surface after the synthesis. However, to improve the Radioluminiscence intensity, an annealing process at 1000 °C was required. The method allows obtaining a nanometric material with a scintillation intensity almost twice higher than that of the commercial powder.

Keywords: Optical materials, chemical synthesis, crystal structure, luminescence, optical spectroscopy

1. Introduction

In recent years, phosphor materials have become more and more attractive for several applications. They are used from cathode ray tubes and plasma display panels to biological labels and luminescence immunoassay, including other fields. Dosimetry in radiotherapy treatments is another possible application of phosphors. Fiber Optic Dosimetry (FOD) is a technique known as an alternative to traditional dosimetry systems. FOD allows in vivo measurements of dose rate, using a small scintillator attached to the end of an optical fiber. The scintillator could be either an organic or inorganic phosphor. When the scintillator is irradiated with high energy beams, the Radioluminescence (RL) emitted is in general proportional to the dose rate absorbed by the phosphor [1].

Despite the particular application, phosphor materials have the singular characteristic of acting as optical transducers: they convert ionizing radiation into visible radiation [2]. When a phosphor material returns to ground state after being excited, it emits radiation with a characteristic wavelength that is related with the identity of the chemical structure. In particular, Rare Earth (RE) elements can work as efficient optical activators of this process. They are used as dopants in different hosts. A RE widely employed as optical activator is Europium, which has a red emission at about 620 nm after excitation if present as Eu^{3+}cation [3].

Vanadates, tungstates, molybdates and other complex oxides are ideal hosts for RE dopants [4]. Among them, Yttrium vanadate, YVO_4, is the typical host for Europium. YVO_4 have a tetragonal zircon type crystalline structure [5]. The atoms are arranged like two distorted tetrahedral, where Yttrium atoms are coordinated by eight Oxygen atoms and Vanadium ones are surrounded by four Oxygen atoms. Doping with Europium generates a substitution process, where Eu^{3+} occupies Y^{3+} sites [2]. Sevic, Rabasovic, Krizan, Savic-Sevic, Mitric, Gilic, Hadzic and Romcevic [6] have reported that doping YVO_4 with Eu^{3+} does not change the crystalline structure of the material, but according to Kumari, Baitha and Manam [4] it might generate changes in the interplanar spacing because Eu^{3+} ionic radius is bigger than Y^{3+} radius.

Since 1964 YVO_4:Eu^{3+} is a red emitter phosphor commercially available as micrometric powder due to its high luminescence efficiency under electron-beam excitation [7]. For this reason, it has been widely employed by industry as red emitter for CRT screens. The feasibility of using YVO_4:Eu^{3+} as FOD detector has been demonstrated by Martínez, Rucci, Marcazzó, Molina, Santiago and Cravero [1], who employed micrometric YVO_4:Eu^{3+} powder to fabricate efficient

scintillators having a volume of 1-3 mm^3. However, no analogous studies for nanometric particles have been carried out so far.

Several reports point out that employing nanometric powder enhances overall scintillation yield by reducing optical scattering losses [8, 9]. Also, enhancement of the scintillation yield of nanometric size phosphors -with respect to micrometric ones- has been reported [10, 11] . The mentioned results make the development of $YVO_4:Eu^{3+}$ based nanoparticle scintillators an issue of interest in the framework of the application of this material to scintillation technology.

The synthesis of $YVO_4:Eu^{3+}$ as nanometric powder has been widely studied by several routes. Uitert, Linares, Soden and Ballman [12] synthesized $YVO_4:Eu^{3+}$ via a solid state reaction. This method has some limitations, such as the lack of homogeneity of the product, the requirement of high annealing temperatures, formation of large particles that have to be milled by mechanical treatments, long times of heat treatments, etc.

In contrast, wet chemical methods are a suitable option for nanoparticle synthesis of $YVO_4:Eu^{3+}$ [2]. Yanhong and Guangyan [13] have reported this synthesis by a traditional coprecipitation method. Huignard, Gacoin and Boilot [14] have studied the same route for colloidal $YVO_4:Eu^{3+}$ nanophosphors. Riwotzki and Haase [15] and Rafiaei and Shokouhimehr [16] synthesized YVO_4 nanoparticles doped with different phosphors by hydrothermal methods. In addition, Ansari and Labis [17] reported the synthesis of nanofibers of $YVO_4:Eu^{3+}$ via an hydrothermal route. Also, the synthesis of Europium doped Yttrium Vanadate using sol-gel methods was studied [18, 19] and novel techniques were reported for the synthesis of this material [20, 21]. However, there are some disadvantages associated with the synthetic techniques mentioned above. For example, coprecipitation method requires high annealing temperature to reach crystallinity in the final product and hydrothermal method demands conditions of high pressures, requiring autoclave reactor.

Combustion route is a simple wet chemical method that requires fuels and oxidizers. It takes place when the mixture of precursors and fuels reaches the auto ignition temperature. Auto ignition temperature is the minimum required temperature at which a fuel in contact with air burns spontaneously. An exothermic reaction is carried out during this process, which under certain conditions could produce a flame.

The required amount of fuels is given by the relationship between oxidizing and reducing components. According to Jain, Adiga and Pai Verneker [22] ϕ_e is defined as the ratio between total amounts of oxidizing elements and reducing elements in the mixture. The combustion could be complete, fuel-rich or lean-rich depending on ϕ_e value. If ϕ_e=1, the reaction is

stoichiometrically balanced and the combustion is complete. In order to minimize damages on environment and avoid production of toxic gases the most suitable option is to work in complete combustion conditions.

Combustion route is a feasible method for the synthesis of luminescent materials, especially for RE doped ones due to its low temperature conditions and short reaction times [2, 23-27]. There are few reports that studied the synthesis of $YVO_4:Eu^{3+}$ via a combustion route. Ekambaram and Patil [28] reported the synthesis of different vanadates doped with Europium (including Yttrium) using ammonium nitrate and 3-methylpyrazole-5-one as fuels. However, they did not report the particle size neither the study of any luminescent property. Kumari, Baitha and Manam [4] studied the synthesis of $YVO_4:Eu^{3+}$ via a combustion route using urea as fuel but they also found a phase of Y_2O_3 in formation. Shokouhimehr and Rafiaei [29] and Rafiaei, Kim and Shokouhimehr [30] compared the effect of different fuels and different solvents in photoluminescence properties and phosphor nanostructure and Rafiaei and Shokouhimehr [31] studied the impact of alumina crucible dimensions in luminescence properties of $YVO_4:Eu^{3+}$. Sevic, Rabasovic, Krizan, Savic-Sevic, Mitric, Gilic, Hadzic and Romcevic [6] reported the formation of $YVO_4:Eu^{3+}$ pure nanoparticles (from 37 to 71 nm) via a combustion route using urea and ammonium nitrate as fuels, but the selected amounts of reagents do not match with those conditions for complete combustion requirements [22].

Recent works have shown efficient cathodoluminescence of sub-micrometer-sized $YVO_4:Eu^{3+}$ samples fabricated by hydrothermal synthesis, which points out the possibility of using $YVO_4:Eu^{3+}$ nanoparticles for ionizing radiation detection [32].

In this work, with the aim of developing a scintillator based on $YVO_4:Eu^{3+}$ nanoparticles suitable for FOD, $YVO_4:Eu^{3+}$ nanoparticles were synthesized employing a combustion method. The reported strategy involves the comparison of the structural and the luminescent properties of $YVO_4:Eu^{3+}$ nanoparticles obtained by the traditional coprecipitation method and combustion route using urea and ammonium nitrate as fuels. The response of the $YVO_4:Eu^{3+}$ nanoparticles to electron irradiation was also evaluated in order to assess the feasibility of using these compounds as detector of ionizing radiation.

2. Material and methods

2.1 Synthesis

YVO_4 nanoparticles were synthesized by two different methods: coprecipitation and combustion route. In both cases, the effect of Eu^{3+} as dopant was studied, so the samples were

synthesized undoped and doped with 5% mol of Eu^{3+}. This concentration has shown to render the most efficient emission of Eu^{3+}doped into this host [33].

Coprecipitation method was reproduced as reported by Yanhong and Guangyan [13]. The starting chemicals were $Y(NO_3)_3.6H_2O$ (Sigma-Aldrich 99,8%), $Eu(NO_3)_3.5H_2O$ (Sigma-Aldrich 99,9%), NH_4VO_3 (Biopack>99%) and NaOH (Anedra 99,3%). For the undoped sample, 40 mL of a NH_4VO_3 solution 0.05 M was adjusted to pH 12.5 with a NaOH solution. 40 mL of a $Y(NO_3)_3$ solution 0.05 M was added dropwise. The mixture was then heated at 60˚ C under magnetic stirring for 1 h. The white opalescent colloid resulting was filtered, washed, dried at 60˚ C and annealed for 2.5 h at 1000˚ C if required. The procedure for the doped sample was analogous, except that instead of using 40 mL of $Y(NO_3)_3$ solution 0.05 M as before, 38 mL of $Y(NO_3)_3$ solution plus 2 mL of $Eu(NO_3)_3$ solution 0.05 M were employed. The chemical reaction involved is shown in **(1)**.

$$(1-x)Y(NO_3)_3 + xEu(NO_3)_3 + NH_4VO_3 \rightarrow Y_{1-x}Eu_xVO_4 \qquad \textbf{(1)}$$

where x=0 for the undoped sample and x=0.05 for the doped sample.

Combustion route was carried out for an oxidizer/fuel ratio equal to 1 [2]. The starting chemicals were $Y(NO_3)_3.6H_2O$ (Sigma-Aldrich 99,8%), $Eu(NO_3)_3.5H_2O$ (Sigma-Aldrich 99,9%), NH_4VO_3 (Biopack>99%); $(NH_2)_2CO$ (Anedra 99%) and NH_4NO_3 (Stanton 99%) as fuels, all of them in analytical grade. The chemical reaction can be symbolized as follows, analogous to that reported by Foka K. E. [34]:

$$(1-x)Y(NO_3)_3 + xEu(NO_3)_3 + NH_4VO_3 + 3(NH_2)_2CO + 3NH_4NO_3 \rightarrow Y_{1-x}Eu_xVO_4 + 14H_2O + 8N_2 + 3CO_2 \qquad \textbf{(2)}$$

where x= 0 for the undoped sample and 0.05 for the doped sample.

For instance, 3.03 g of $Y(NO_3)_3.6H_2O$, 0.18 g of $Eu(NO_3)_3.5H_2O$, 0.97 g of NH_4VO_3, 1.50 g of $(NH_2)_2CO$ and 2.00 g of NH_4NO_3 were separately dissolved in distilled water. Each solution was slowly added to the $Y(NO_3)_3$ solution. The resulting yellow solution was then concentrated by heating at 70 ˚C under magnetic stirring until free water evaporated. Then, the as-prepared red gel was heated at 200˚C in a heating mantle for 2 h until the combustion was completed. A foamy orange powder was obtained and certain fractions were annealed at 600, 800 or 1000 ˚C for 2.5 h. For the undoped sample the proceeding was analogous, all amounts were the same except that of $Y(NO_3)_3.6H_2O$, which was 3.19 g.

2.2 Characterization techniques

X-Ray Diffraction (XRD) analysis of the samples were carried out on a Philips 3020 diffractometer with CuKα radiation (λ = 1,54 Å) and Ni filter at 34 kV and 40 mA. All patterns were recorded in the 2θ range from 15˚ to 70˚ with a step size of Δ2θ= 0,04˚.

Fourier Transform Infrared Spectroscopy (FTIR) data were obtained on a Nicolet Magna 550 spectrometer with Nernst filament source, Germanium film with ICs beamsplitter and DTGS pyroelectric detector. The patterns were obtained from 400 cm^{-1} to 4000 cm^{-1} at a resolution of 4 cm^{-1} after making pellets of the samples diluted in KBr via hydraulic press machine.

TEM images were taken in a transmission electron microscope Jeol JEM 2100 with B6La filament at 200 kV. These images were processed using Image J software and the histograms for particle sizes were carried out in Origin Pro 8.

Thermogravimetric Analysis (TGA) of the nanoparticles were performed in a Q500 TA Instrument thermogravimetric analyzer. Tests were carried out at a heating rate of 10 °C/min from 30 to 900 °C in air atmosphere. The samples were about 10 mg in all cases.

The excitation and emission spectra were obtained in a Varian Cary Eclipse fluorescence spectrophotometer. Measurements were recorded at a scan rate of 600 nm/min and with a spectral resolution of 5 nm. The Decay times of the luminescence signals were also investigated. The samples were excited with UV pulses (266 nm) from the fourth harmonic of a Continuum Surelite II Nd:YAG pulsed laser. The light coming from the sample was filtered to get rid of spectral components having wavelength shorter than 520 nm. Luminescence was detected by means of a Hamamatsu-H7360-03 photon counting head. The emission light was recorded for 60 seconds at a pulse frequency of 10 Hz. Pulses were averaged and fitted with a two-component exponential decay function to obtain characteristic lifetimes (τ_1 and τ_2) of the UV-excited emission.

Radioluminescence (RL) measurements were carried out to assess the scintillation yield of each sample. The results were compared with those from a commercial sample of $YVO_4:Eu^{3+}$ kindly provided by Phosphor Technology Ltd. (United Kingdom). Commercial powder has an average particle size of 5 µm (according to the manufacturer specifications). Samples were irradiated at room temperature by resorting to a 10 mCi ophthalmic 90Sr beta-source rendering a dose rate of 0.022 Gy/min at the sample position. The intensity of the scintillation light was recorded with a Hamamatsu H7360-03 photon counting head. This light detector has a spectral window ranging from 300 up to 850 nm.

3. Results and discussion

3.1 Structure characterization

XRD measurements were performed on the nanoparticles to extract information about their crystalline structure.

Figure 1 shows the diffraction profiles recorded for the undoped nanoparticles synthesized by coprecipitation method and combustion route. For both cases, patterns corresponding to the as-synthesized nanoparticles and after annealing at 1000˚C are shown. As can be seen, the as-synthesized nanoparticles show broad diffraction peaks and weak signals, typical of low crystallinity nanoparticles. In contrast, the annealed nanoparticles exhibit narrow and more intense diffraction peaks, indicating an improvement in crystallinity due to the annealing. For identification purpose, these patterns were compared with those reported in the Crystallography Open Database (COD). A single crystalline phase is identified in combustion nanoparticles which corresponds to YVO_4 (9009764 COD). Instead, two crystalline phases were identified in coprecipitation nanoparticles, Y_2O_3 and YVO_4. The crystalline phase corresponding to Y_2O_3 was identified by the diffraction peak at $2\theta = 29.2^{\circ}$ assigned to the reflections from the (222) plane of the Y_2O_3 crystal lattice (1009015 COD). Semiquantitative analysis results are 95% YVO_4 and 5% Y_2O_3.

Figure 2 compares the XRD patterns of doped and undoped samples synthesized by coprecipitation method after annealing at 1000 ˚C. The doped nanoparticles show three crystalline phases identified as YVO_4, Y_2O_3 and Eu_2O_3 according to reported in COD. In addition, the highest intensity peak corresponds to Y_2O_3, indicating that this is the crystalline phase that is present in the highest proportion (semiquantitative analysis results are 52% Y_2O_3, 26% Eu_2O_3 and 22% YVO_4). Attending that the main objective of this work is the synthesis of doped YVO_4 due to its subsequent technological application as scintillator nanoparticles suitable for FOD, the focus will be centered on the nanoparticles obtained by combustion synthesis.

Figure 3 shows XRD patterns of doped nanoparticles synthesized by combustion route (as-synthesized and annealed at 1000˚C) and, as reference, the pattern corresponding to the undoped nanoparticles annealed at 1000˚C. All diffraction peaks are in good agreement to those reported in COD for YVO_4 structure. No additional peaks that could suggest the presence of another crystalline phase in doped samples are observed. This is strong evidence that can justify the substitution of Y^{3+} by Eu^{3+} into YVO_4 structure [6]. It can be observed that peak positions in doped samples are slightly shifted towards lower 2θ values. According to Kumari, Baitha and Manam [4], it could be due to the higher ionic radius of Eu^{3+} with respect to Y^{3+}. It

would increase crystalline network size and consequently the crystallite size, D, whose value can be calculated using Scherrer equation [35]:

$$D = \frac{K\lambda}{B\cos\theta} \quad \textbf{(3)}$$

where K is a factor related to crystallite shape (0,9 is generally a good approximation), B the width of the X-ray diffraction peak in radians, λ the X-ray wavelength (0,15405 nm) and θ de diffraction angle. According to maximum intensity peak, the estimated crystallite sizes are listed in Table 1. The increment in the values of "D" also highlights the effect of annealing on crystallinity.

Sample	Annealing temperature	D (nm)
YVO_4	-	24
YVO_4	1000˚ C	43
$Y_{0,95}Eu_{0,05}VO_4$	-	31
$Y_{0,95}Eu_{0,05}VO_4$	1000˚ C	54

Table 1.Crystallite size (D) estimated by Scherrer equation.

3.2 Morphological characterization

Figure 4 shows TEM images of the nanoparticles synthesized by combustion route. In all of them, it can be clearly seen that nanoparticles are agglomerated. In as-synthesized samples a) and c), the nanoparticles present low crystallinity (attending to XRD data previously shown) but have an apparently homogenous morphology. In annealed samples b) and d), the nanoparticles are bigger, with an improved crystallinity but with a more heterogeneous morphology. These images put on evidence that the annealing promotes coalescence and aggregation processes that increase nanoparticle size and result in more polyhedral shapes.

Figure 5 shows histograms of the nanoparticle size calculated by TEM image analysis. Starting with the undoped samples, 96% of as-synthesized nanoparticles (histogram (a)) have particle sizes below 14 nm, 52% of them are in the range of 6-10 nm. In the case of the annealed nanoparticles (histogram (b)), 95% of the nanoparticles have particle sizes lower than 250 nm with a 51% of them comprised between 100-150 nm. The analysis clearly shows the effect of heat treatment on increasing particle size.

Analogously for doped samples, 95% of as-synthesized nanoparticles (histogram (c)) have particle sizes lower than 14 nm with a 52% of them comprised between 6-10 nm. According to

histogram (d), after the annealing, 79% of the nanoparticles have particle sizes lower than 250 nm while 55% of them are in the range of 50-200 nm.

From the comparison between annealed nanoparticles (doped and undoped), it is noted that the maximum particle size registered for the undoped nanoparticles was around 400 nm meanwhile for the doped nanoparticles (synthesized under the same conditions) it was significantly higher, around 550 nm.

The differences observed between the values obtained for the crystallite size (D, Table 1) and for the particle size (calculated from TEM images) can be justified based on the dislocations and defects present in the structures of the nanoparticles. These two parameters would have the same value in the ideal case in which the grains were simple perfect crystals. In the present case, TEM images show agglomeration and several defects that interrupt the periodicity of the crystalline structure. Therefore, an individual particle may contain a number of crystallites defined as coherently diffracting regions [36, 37].

3.3 Surface Characterization

FTIR spectra for $YVO_4:Eu^{3+}$ nanoparticles synthesized by coprecipitation and combustion methods after annealing are shown in Figure 6. Combustion sample presents two characteristic bands. The intense band observed around 812 cm^{-1} is characteristic of V-O bond vibration, particularly of VO_4^{3-} group. Another band with lower intensity is located around 453 cm^{-1}. It is associated with the vibration of the Y-O bond [4, 38]. There are no evidences that suggest that the sample could have any impurity adsorbed on the surface. Considering XRD data shown previously, it can be concluded that $YVO_4:Eu^{3+}$ nanoparticles obtained by combustion route after annealing correspond to a pure compound.

On the other hand, FTIR spectrum of coprecipitation nanoparticles shows at least four characteristic bands. The two located around 839 and 476 cm^{-1} are characteristic of V-O and Y-O bond vibrations, respectively. There is another band near 766 cm^{-1} that can be attributed to N-O bond vibration corresponding to some precursor that could have been adsorbed on the surface [39]. As XRD data showed, this sample has three crystalline phases: YVO_4, Y_2O_3 and Eu_2O_3 with yttrium oxide in majority. In FTIR spectrum of coprecipitation sample, the most intense band is the one located in 476 cm^{-1} (in combustion sample is the one located in 812 cm^{-1}). It could indicate that there are more Y-O bonds that increase the intensity of the band, due to the presence of Y_2O_3 crystalline phase. However, FTIR analysis does not show any evidence

of Eu_2O_3 formation, probably because Eu-O bonds have characteristic vibrations that appear at frequencies lower than 400 cm^{-1}[40].

Figure 7 shows FTIR spectra of YVO_4 nanoparticles obtained by combustion route. There are five characteristic bands in the as-synthesized sample. The two located around 812 y 453 cm^{-1} are attributed to V-O and Y-O bond vibration respectively. The broad peak near 3410 cm^{-1} could be assigned to O-H stretching vibrations and the one located around 1640 cm^{-1} to O-H bending vibrations [38]. The band near 1380 cm^{-1} is characteristic of C-O bending vibrations [4]. There could be another peak not well defined around 1310 cm^{-1} associated with the presence of NO_3^- group vibration [41]. Therefore, there are impurities associated with precursors that might be adsorbed on nanoparticle surface. Figure 7 also shows the spectra corresponding to the annealed samples at two different temperatures (600 and 1000 °C) in order to evaluate the effect of annealing temperature on the nanoparticles composition. As can be seen, impurity bands almost disappear in FTIR spectra as the annealing temperature increases, likely due to temperature-activated surface degradation processes. Furthermore, there are no significant differences between doped and undoped FTIR spectra after annealing at 1000 ˚C. It could indicate that the presence of Eu^{3+} does not change the composition of the nanoparticles surface.

3.4 Thermal Characterization

In order to contrast the data obtained through FTIR spectra, a Thermogravimetric Analysis (TGA) of the as-synthesized YVO_4:Eu^{3+} nanoparticles obtained by combustion route was carried out (Figure 8). As can be seen, the mass loss takes place in two consecutive steps. The first occurs between 100-200 ˚C, showing a 5% mass loss. It is immediately followed by the second step comprised between 250-550˚C, which has a lower slope. About 10% of initial mass is lost between these two steps. After that, it seems to be only slight changes in the nanoparticles mass.

Considering also FTIR data, the mass loss shown by TGA data could be due to superficial changes, in particular, to the degradation of impurities that remained adsorbed on surface immediately after reaction.

3.5 Luminescence properties

Figure 9 shows the emission spectra (λex=271 nm) of YVO_4:Eu^{3+} corresponding to the commercial sample (red line) and the combustion sample annealed at 1000°C (black line) normalized with respect to sample weight. The shapes of both spectra fairly match. The

observed emission peaks can be assigned to characteristic transitions of Eu^{3+} cation. In particular, peaks located at 590, 618, 652 and 699 nm are characteristic of $^5D_0 \rightarrow ^7F_J$ (J=1, 2, 3, 4) transitions. Luminescence from higher excited states of Eu^{3+} can also be identified, namely, peaks at 555 and 595 nm corresponding to $^5D_1 \rightarrow ^7F_2$ and $^5D_1 \rightarrow ^7F_3$ transitions, respectively [4, 11]. The prominence of the emission corresponding to the $^5D_0 \rightarrow ^7F_2$ transition with respect to the intensity of the peak assigned to the $^5D_0 \rightarrow ^7F_1$ transition demonstrates that Eu^{3+} cations occupy sites having low inversion [19]. The presence of $^5D_1$ emission peaks can be possible by taking into account that the vibration energy of VO_4^{3-} groups is not high enough to depopulate the $^5D_1$ states through the $^5D_0$ level [19]. It is also apparent from Figure 9 that $YVO_4:Eu^{3+}$ nanoparticles emit more efficiently than micrometric powder under UV excitation. This effect has been also observed in many other phosphors and could be related to the confinement of the longer lifetime excitation of Eu^{3+} within the nanoparticles [11, 42, 43]. Indeed, the decay lifetimes of the $YVO_4:Eu^{3+}$combustion nanoparticles annealed at 1000°C are slightly higher than those corresponding to the commercial sample, as can be seen from Table 2. As can be seen from the table, two exponential decaying signals had to be assumed to consistently fit the experimental data. The values obtained are fairly similar to previous reports, which demonstrates efficient synthesis of $YVO_4:Eu^{3+}$ nanoparticles [32].

Sample	τ_1 (s)	τ_2 (s)
Commercial $YVO_4:Eu^{3+}$	0.0117 ± 0.0002	0.0633 ± 0.0001
Combustion $YVO_4:Eu^{3+}$(1000°C)	0.0128 ± 0.0001	0.0707 ± 0.0002

Table 2: Decay lifetimes of the photoluminescence signal of the commercial sample and of $YVO_4:Eu^{3+}$ nanoparticles synthesized by the combustion method after annealing at 1000°C.

The dependence of the scintillation yield of the $YVO_4:Eu^{3+}$ combustion sample as function of the annealing temperature is shown in Figure 10. The RL signal has been normalized to the RL emission of the commercial sample. Maximum relative scintillation is attained after annealing the sample at 1000°C, being the scintillation intensity of this sample almost twice higher than that of the commercial powder. The scintillation signal of the most efficient $YVO_4:Eu^{3+}$ combustion sample, namely, the sample annealed at 1000°C is compared to that from the commercial sample (Figure 11). Both signals have shown to be stable and repetitive along the irradiation time. The enhancement of the luminescence as the sample is annealed at higher temperature is probably related to the better crystallinity and phase purity achieved by the thermal treatment [32, 44].

According to FTIR and TGA data, there are impurities adsorbed on nanoparticles surface that remain after combustion synthesis. These impurities could provide non-radiative paths to relaxation. These compounds are eliminated when annealing temperature increases, as confirmed by TGA analysis. At the same time higher crystallinity is attained, so improving the scintillation efficiency.

From emission spectra it is possible to calculate the chromaticity coordinate values of CIE 1931 Diagram. $YVO_4:Eu^{3+}$ is a red-emitting phosphor so their coordinates are around this region of CIE Diagram. As seen in Figure 12, both commercial and combustion samples have almost the same coordinates (x=0,63 and y=0,37), which are similar to those previously reported [4, 6].

The particles synthesized by the combustion method have high crystallinity, an homogenous morphological distribution and nanometric particle sizes. In turn, the synthesis method is simple, fast and does not require sophisticated equipment. The luminescent behavior is promising for its application as a scintillator in the technological design of new composite materials for FOD. In a next stage the development of a composite material will be carried out to be used as a sensor at the ends of an optical fiber.

4. Conclusions

In order to synthesize $YVO_4:Eu^{3+}$ nanoparticles a thorough analysis of two different preparation methods, namely, coprecipitation and combustion routes, was carried out. Nominally pure and Europium doped samples were obtained in order to evaluate crystalline structural changes when Eu^{3+} replaces Y^{3+}cation into the YVO_4 host.

In the sample prepared by coprecipitation, two different crystalline phases were obtained (yttrium oxide and yttrium vanadate). Probably due to the coexistence of multiple phases and related quenching effects of radiation-induced luminescence, the RL intensity of this sample was almost undetectable.

In contrast, a unique crystalline phase was obtained when the combustion route was employed for the preparation. In this case, particle size ranges from 55 up to 200 nm. FTIR and TGA analysis indicated that annealing at 600°C promote the degradation of the impurities that remain adsorbed on nanoparticles surface after synthesis. However, to improve the RL intensity, it was necessary to anneal the nanocrystalline powder at 1000°C. After this thermal treatment, RL intensity of this sample was almost twice higher than that of the commercial microcrystalline sample. Emission spectra under UV excitation are characteristic of f-f

electronic transitions of Eu^{3+}cation. CIE 1931 Diagram indicates that combustion sample have the same coordinates than commercial $YVO_4:Eu^{3+}$.

Combustion route is a technically simple and inexpensive synthesis method to obtain $YVO_4:Eu^{3+}$ nanoparticles, which could be employed to develop suitable scintillators for Fiber Optic Dosimetry due to their good structural and optical properties.

Acknowledgement

The authors would also like to acknowledge the assistance by the technical expertise provided by Dr. Marcelo Ceolín (INIFTA – Argentine).

I.A.Z., M.S., and G.B. are members of the Carrera del Investigador Cientifico y Tecnológico, CONICET, Argentine. L.M and N.M. are research fellows of CONICET, Argentine.

This work was supported by Agencia Nacional de Promoción Científica y Tecnológica (PICT 2015-1555); Consejo Nacional de Investigaciones Científicas y Técnicas (PIP 2015-800 and PIP 2015-844) and Universidad Nacional del Centro de la Provincia de Buenos Aires (PIO-30C).

References

[1] N. Martínez, A. Rucci, J. Marcazzó, P. Molina, M. Santiago, W. Cravero, Characterization of YVO4:Eu3+ scintillator as detector for Fiber Optic Dosimetry, Radiation Measurements, 106 (2017) 650-656.
[2] S. Ekambaram, K.C. Patil, M. Maaza, Synthesis of lamp phosphors: facile combustion approach, Journal of Alloys and Compounds, 393 (2005) 81-92.
[3] Y.W.M. Shionoya Shigeo, Yamamoto Hajime, Phosphor Handbook, 2nd ed., CRC Press, 2006.
[4] P. Kumari, P.K. Baitha, J. Manam, Structural and photoluminescence properties of red-light emitting YVO4:Eu3+ phosphor synthesized by combustion and solid-state reaction techniques: a comparative study, Indian Journal of Physics, 89 (2015) 1297-1306.
[5] J.A. Baglio, G. Gashurov, A refinement of the crystal structure of yttrium vanadate, Acta Crystallographica Section B, 24 (1968) 292-293.
[6] D. Sevic, M.S. Rabasovic, J. Krizan, S. Savic-Sevic, M. Mitric, M. Gilic, B. Hadzic, N. Romcevic, Characterization and luminescence kinetics of Eu3+ doped YVO4 nanopowders, Materials Research Bulletin, 88 (2017) 121-126.
[7] N. Vu, T. Chi, D. Nguyen, Combustion synthesis and characterization of Er3+-doped and Er3+, Yb3+-codoped YVO4 nanophosphors oriented for luminescent biolabeling applications, 2011.
[8] Z. Kang, M. Barta, J. Nadler, B. Wagner, R. Rosson, B. Kahn, Synthesis of BaF2:Ce nanophosphor and epoxy encapsulated transparent nanocomposite, Journal of Luminescence, 131 (2011) 2140-2143.
[9] T.J. Hajagos, C. Liu, N.J. Cherepy, Q. Pei, High-Z Sensitized Plastic Scintillators: A Review, Advanced Materials, 30 (2018) 1706956.
[10] Y. Iso, S. Takeshita, T. Isobe, Fabrication and characterization of transparent monolithic nanocomposites between YVO4:Bi3+,Eu3+ nanophosphor and TMAS-derived silica, Optical Materials, 36 (2014) 717-722.

[11] W.-T. Hsu, W.-H. Wu, C.-H. Lu, Synthesis and luminescent properties of nano-sized Y3Al5O12:Eu3+ phosphors, Materials Science and Engineering: B, 104 (2003) 40-44.
[12] L.G.V. Uitert, R.C. Linares, R.R. Soden, A.A. Ballman, Role of f-Orbital Electron Wave Function Mixing in the Concentration Quenching of Eu3+, The Journal of Chemical Physics, 36 (1962) 702-705.
[13] L. Yanhong, H. Guangyan, Synthesis and luminescence properties of nanocrystalline YVO4:Eu3+, Journal of Solid State Chemistry, 178 (2005) 645-649.
[14] A. Huignard, T. Gacoin, J.-P. Boilot, Synthesis and Luminescence Properties of Colloidal YVO4:Eu Phosphors, Chemistry of Materials, 12 (2000) 1090-1094.
[15] K. Riwotzki, M. Haase, Wet-Chemical Synthesis of Doped Colloidal Nanoparticles: YVO4:Ln (Ln = Eu, Sm, Dy), The Journal of Physical Chemistry B, 102 (1998) 10129-10135.
[16] S.M. Rafiaei, M. Shokouhimehr, Synthesis and luminescence properties of transparent YVO4: Eu3+ phosphors, Materials Research Express, 5 (2018) 116208.
[17] A.A. Ansari, J.P. Labis, Preparation and photoluminescence properties of hydrothermally synthesized YVO4:Eu3+ nanofibers, Materials Letters, 88 (2012) 152-155.
[18] A. Luo, G. Du, H. Lai, W. Shi, Photoluminescence of europium-doped and europium/strontium-codoped sol–gel-prepared yttrium vanadate nanoparticles, Materials Science in Semiconductor Processing, 23 (2014) 20-26.
[19] S.M. Rafiaei, T.D. Isfahani, H. Afshari, M. Shokouhimehr, Improved optical properties of YVO4:Eu3+ nano–layers on silica spheres, Materials Chemistry and Physics, 203 (2018) 274-279.
[20] K. Uematsu, K. Toda, M. Sato, Preparation of YVO4:Eu3+ phosphor using microwave heating method, Journal of Alloys and Compounds, 389 (2005) 209-214.
[21] H. Yu, Y. Song, Y. Li, Y. Wu, B. Chen, P. Li, C. Sheng, Preparation and luminescent properties of one-dimensional YVO4:Eu nanocrystals, Journal of Materials Science: Materials in Electronics, 27 (2016) 2608-2613.
[22] S.R. Jain, K.C. Adiga, V.R. Pai Verneker, A new approach to thermochemical calculations of condensed fuel-oxidizer mixtures, Combustion and Flame, 40 (1981) 71-79.
[23] S. Rafiaei, A. Kim, M. Shokouhimehr, Enhanced luminescence Properties of Combustion Synthesized Y2O3:Gd Nanostructure, Current Nanoscience, 11 (2015).
[24] M. Venugopal, H.P. Kumar, R. Satheesh, R. Jayakrishnan, Effect of annealing temperature in the emission properties of nanocrystalline CaZr0.9SmxDy0.1−xO3 systems prepared via self-propagating combustion synthesis, Physics Letters A, (2020) 126280.
[25] S. Shi, Y. Yang, P. Guo, J. Wang, L. Geng, L. Fu, Improved morphology and optimized luminescence of Eu3+-doped La2Ce2O7 composite nanopowders by surfactant-assisted solution combustion synthesis, Journal of Luminescence, 206 (2019) 91-96.
[26] R.K. Tamrakar, D.P. Bisen, K. Upadhyay, N. Bramhe, Down-conversion luminescence property of Er3+ and Yb3+ co-doped Gd2O3 crystals prepared by combustion synthesis and solid state reaction method, Superlattices and Microstructures, 81 (2015) 34-48.
[27] S.M. Rafiaei, M. Shokouhimehr, Effect of fuels on nanostructure and luminescence properties of combustion synthesized MgAl2O4:Eu3+ phosphors, Journal of Molecular Structure, 1193 (2019) 274-279.
[28] S. Ekambaram, K.C. Patil, Rapid synthesis and properties of FeVO4, AlVO4, YVO4 and Eu3+-doped YVO4, Journal of Alloys and Compounds, 217 (1995) 104-107.
[29] M. Shokouhimehr, S.M. Rafiaei, Combustion synthesized YVO4:Eu3+ phosphors: Effect of fuels on nanostructure and luminescence properties, Ceramics International, 43 (2017) 11469-11473.
[30] S. Rafiaei, A. Kim, M. Shokouhimehr, Effect of Solvent on Nanostructure and Luminescence Properties of Combustion Synthesized Eu3+ Doped Yttria, Nanoscience and Nanotechnology Letters, 6 (2014) 692.

[31] S.M. Rafiaei, M. Shokouhimehr, Impact of process parameters on luminescence properties and nanostructure of YVO4:Eu phosphor, Materials Chemistry and Physics, 229 (2019) 431-436.
[32] F. He, P. Yang, N. Niu, W. Wang, S. Gai, D. Wang, J. Lin, Hydrothermal synthesis and luminescent properties of YVO4:Ln3+ (Ln=Eu, Dy, and Sm) microspheres, Journal of Colloid and Interface Science, 343 (2010) 71-78.
[33] A. Huignard, V. Buissette, A.-C. Franville, T. Gacoin, J.-P. Boilot, Emission Processes in YVO4:Eu Nanoparticles, The Journal of Physical Chemistry B, 107 (2003) 6754-6759.
[34] D.B.F. Foka K. E., Swart H. C., Combustion Synthesis of Dy3+ –doped YVO4 phosphor, in: Proceedings of SAIP2014, University of Johannesburg, Johannesburg, 2014, pp. 34-40.
[35] U. Holzwarth, N. Gibson, The Scherrer equation versus the 'Debye-Scherrer equation&#39, Nature Nanotechnology, 6 (2011) 534.
[36] S.H. Chamola Arun, Naithani U.C., Study Of Pb(Zr0.65Ti0.35)O3(PZT(65/35) Doping On Structural, Dielectric And Conductivity Properties Of BaTiO3(BT) Ceramics, Advanced Materials Letters, 2 (2011) 5.
[37] P. Goel, K.L. Yadav, Substitution site effect on structural and dielectric properties of La–Bi modified PZT, Journal of Materials Science, 42 (2007) 3928-3935.
[38] M.N. Luwang, R.S. Ningthoujam, S.K. Srivastava, R.K. Vatsa, Preparation of white light emitting YVO4: Ln3+ and silica-coated YVO4:Ln3+ (Ln3+ = Eu3+, Dy3+, Tm3+) nanoparticles by CTAB/n-butanol/hexane/water microemulsion route: Energy transfer and site symmetry studies, Journal of Materials Chemistry, 21 (2011) 5326-5337.
[39] R. Srinivasan, N.R. Yogamalar, J. Elanchezhiyan, R.J. Joseyphus, A.C. Bose, Structural and optical properties of europium doped yttrium oxide nanoparticles for phosphor applications, Journal of Alloys and Compounds, 496 (2010) 472-477.
[40] J.-C. Bünzli, E. Moret, J.R. Yersin, Vibrational Spectra of Anhydrous Lanthanum, Europium, Gadolinium, and Dysprosium Nitrates and Oxinitrates, 1978.
[41] H. Zhang, X. Fu, S. Niu, Q. Xin, Synthesis and luminescent properties of nanosized YVO4:Ln (Ln=Sm, Dy), Journal of Alloys and Compounds, 457 (2008) 61-65.
[42] G. Wakefield, H.A. Keron, P.J. Dobson, J.L. Hutchison, Synthesis and Properties of Sub-50-nm Europium Oxide Nanoparticles, Journal of Colloid and Interface Science, 215 (1999) 179-182.
[43] Y.-S. Chang, F.-M. Huang, Y.-Y. Tsai, L.-G. Teoh, Synthesis and photoluminescent properties of YVO4:Eu3+ nano-crystal phosphor prepared by Pechini process, Journal of Luminescence, 129 (2009) 1181-1185.
[44] G.S. Ningombam, T.S. David, N.R. Singh, Enhancement of Eu3+ Emission in YVO4:Eu3+ Nanocrystals by Li+ Codoping: An Oxidant-Resistant Dispersion and Polymer Film, ACS Omega, 4 (2019) 13762-13771.

Figure Captions

Figure 1. XRD patterns of undoped samples synthesized via coprecipitation method and combustion route.

Figure 2. XRD patterns of coprecipitation YVO_4 samples.

Figure 3. XRD patterns of combustion YVO_4 samples.

Figure 4. TEM images of YVO_4 samples. **a)** undoped, as-synthesized **b)** undoped, annealed at 1000˚C **c)** doped, as-synthesized **d)** doped, annealed at 1000˚C

Figure 5.Size histograms for YVO_4 samples. **a)** undoped, as-synthesized **b)** undoped, annealed at 1000˚C **c)** doped, , as-synthesized **d)** doped, annealed at 1000˚C

Figure 6. FTIR analysis for $YVO_4:Eu^{3+}$ samples.

Figure 7. FTIR spectra of $YVO_4:Eu^{3+}$ combustion samples.

Figure 8.Thermogravimetric Analysis for $YVO_4:Eu^{3+}$ combustion sample.

Figure 9. Emission spectra of $YVO_4:Eu^{3+}$ samples excited at 271 nm

Figure 10. RL intensity of $YVO_4:Eu^{3+}$sample synthesized by combustion route at different annealing temperatures, normalized to the RL of the commercial sample.

Figure 11. Radioluminescence signal from the $YVO_4:Eu^{3+}$ sample annealed at 1000°C and the commercial sample.

Figure 12. CIE 1931 Diagram

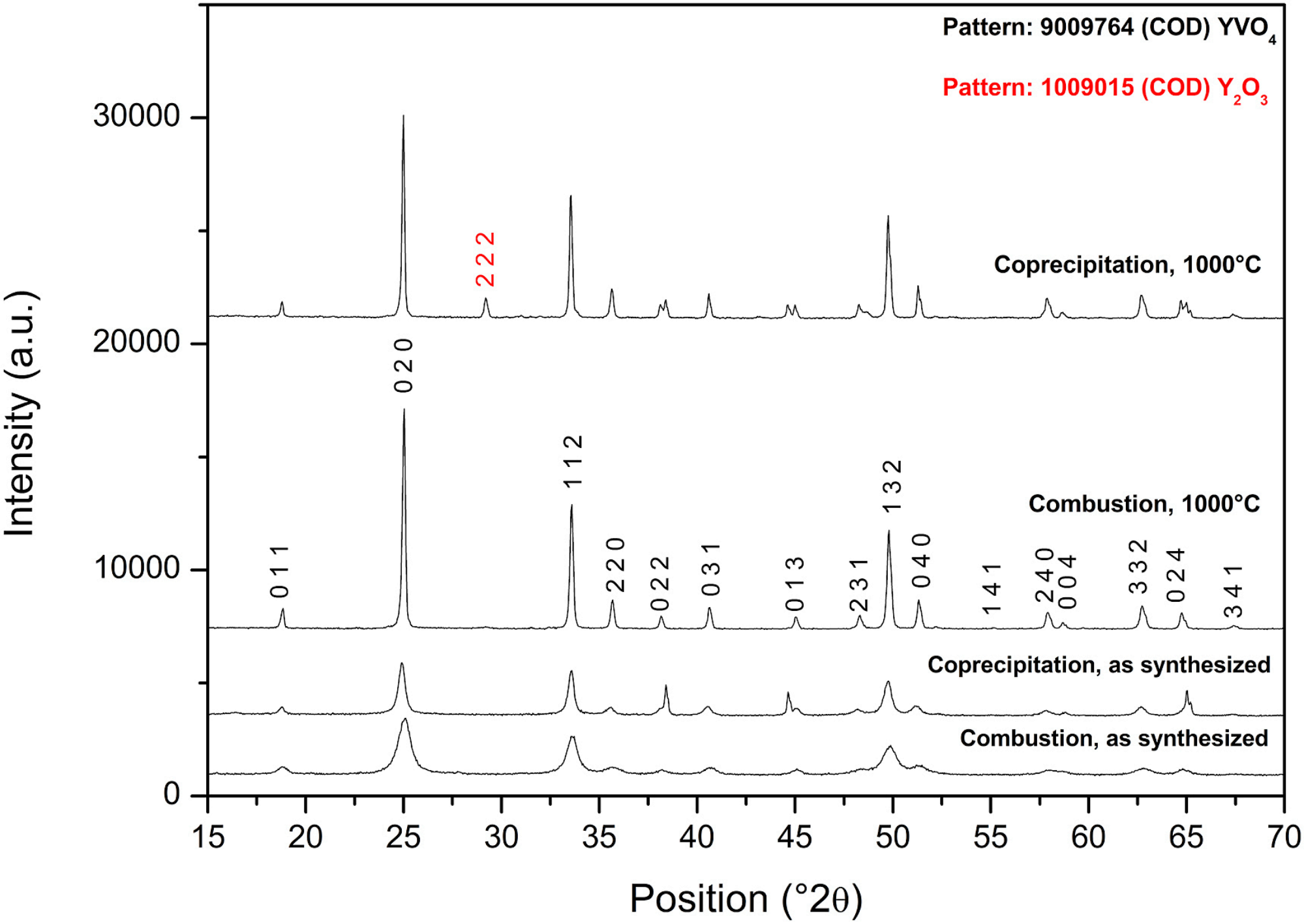
Pattern: 9009764 (COD) YVO4
Pattern: 1009015 (COD) Y2O3
Coprecipitation, 1000°C
Combustion, 1000°C
Coprecipitation, as synthesized
Combustion, as synthesized
222
020
112
220
022
031
013
231
132
040
141
240
004
332
024
341
011
Intensity (a.u.)
Position (°2θ)
0
10000
20000
30000
15
20
25
30
35
40
45
50
55
60
65
70

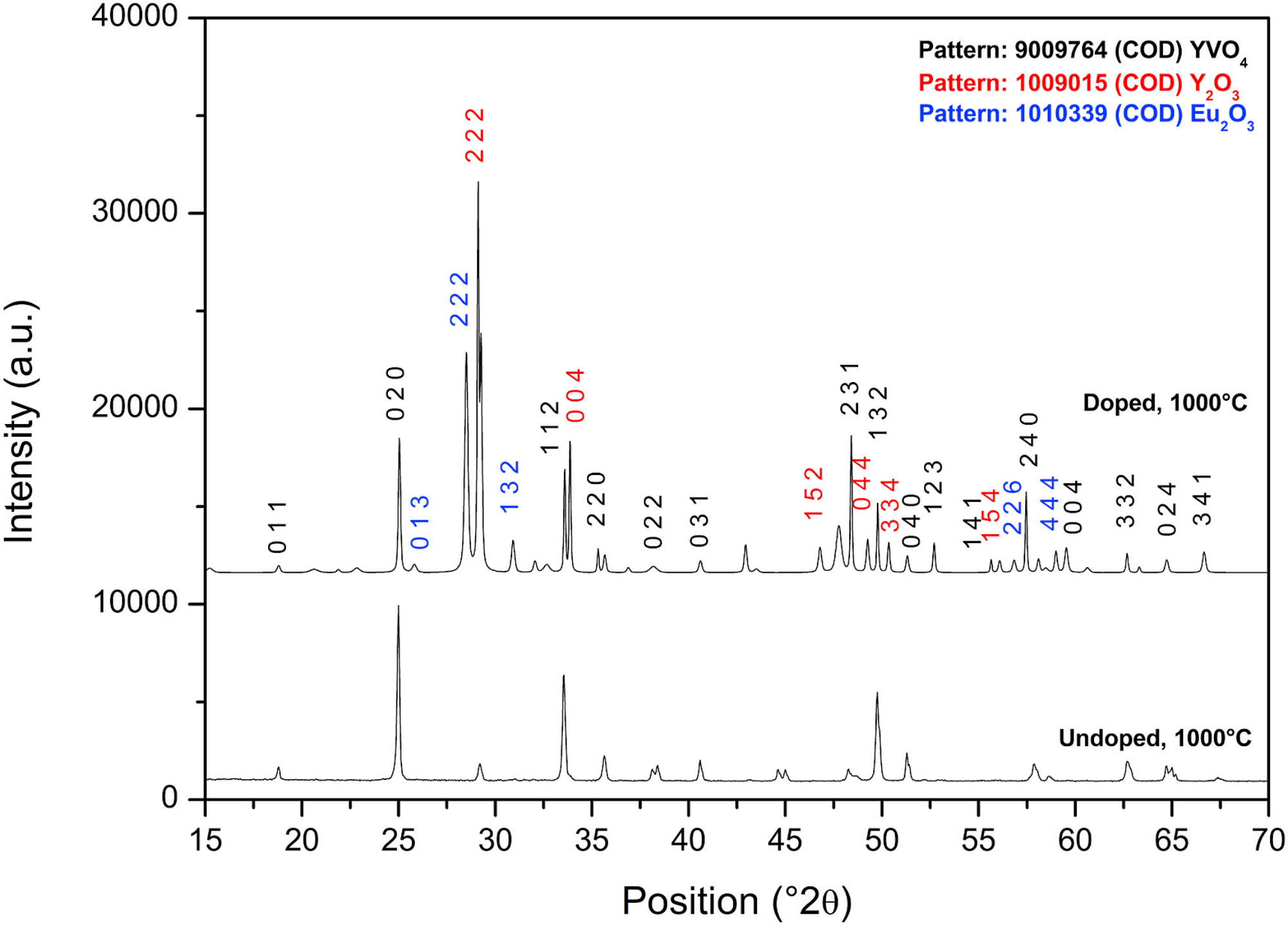
Pattern: 9009764 (COD) YVO4
Pattern: 1009015 (COD) Y2O3
Pattern: 1010339 (COD) Eu2O3
Doped, 1000°C
Undoped, 1000°C
Intensity (a.u.)
Position (°2θ)
0
10000
20000
30000
40000
15
20
25
30
35
40
45
50
55
60
65
70
011
020
013
222
222
132
112
004
220
022
031
152
231
132
044
334
040
123
141
154
226
240
444
004
332
024
341

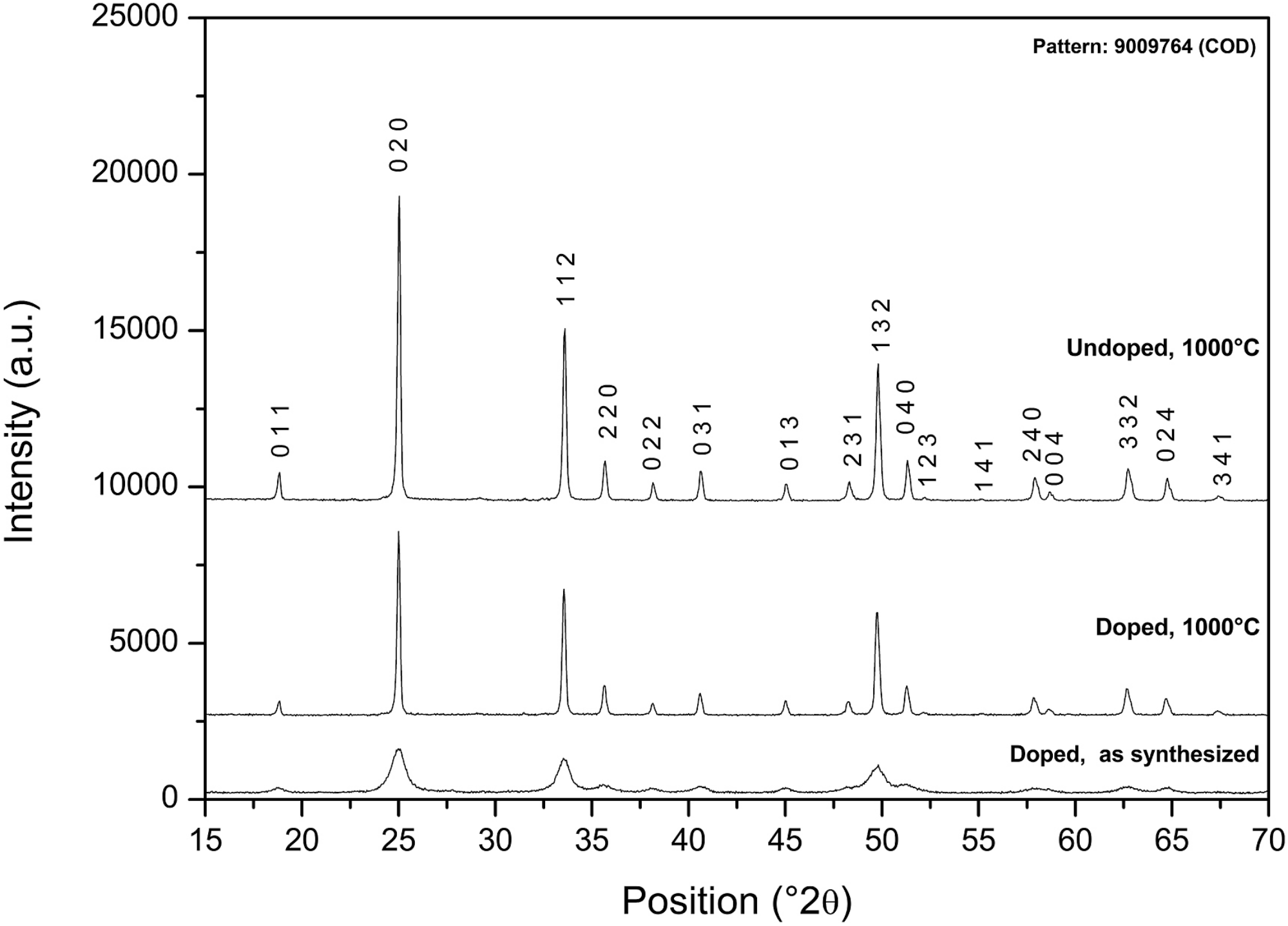
Pattern: 9009764 (COD)
Undoped, 1000°C
Doped, 1000°C
Doped, as synthesized
0 1 1
0 2 0
1 1 2
2 2 0
0 2 2
0 3 1
0 1 3
2 3 1
1 3 2
0 4 0
1 2 3
1 4 1
2 4 0
0 0 4
3 3 2
0 2 4
3 4 1
Intensity (a.u.)
Position (°2θ)
25000
20000
15000
10000
5000
0
15
20
25
30
35
40
45
50
55
60
65
70

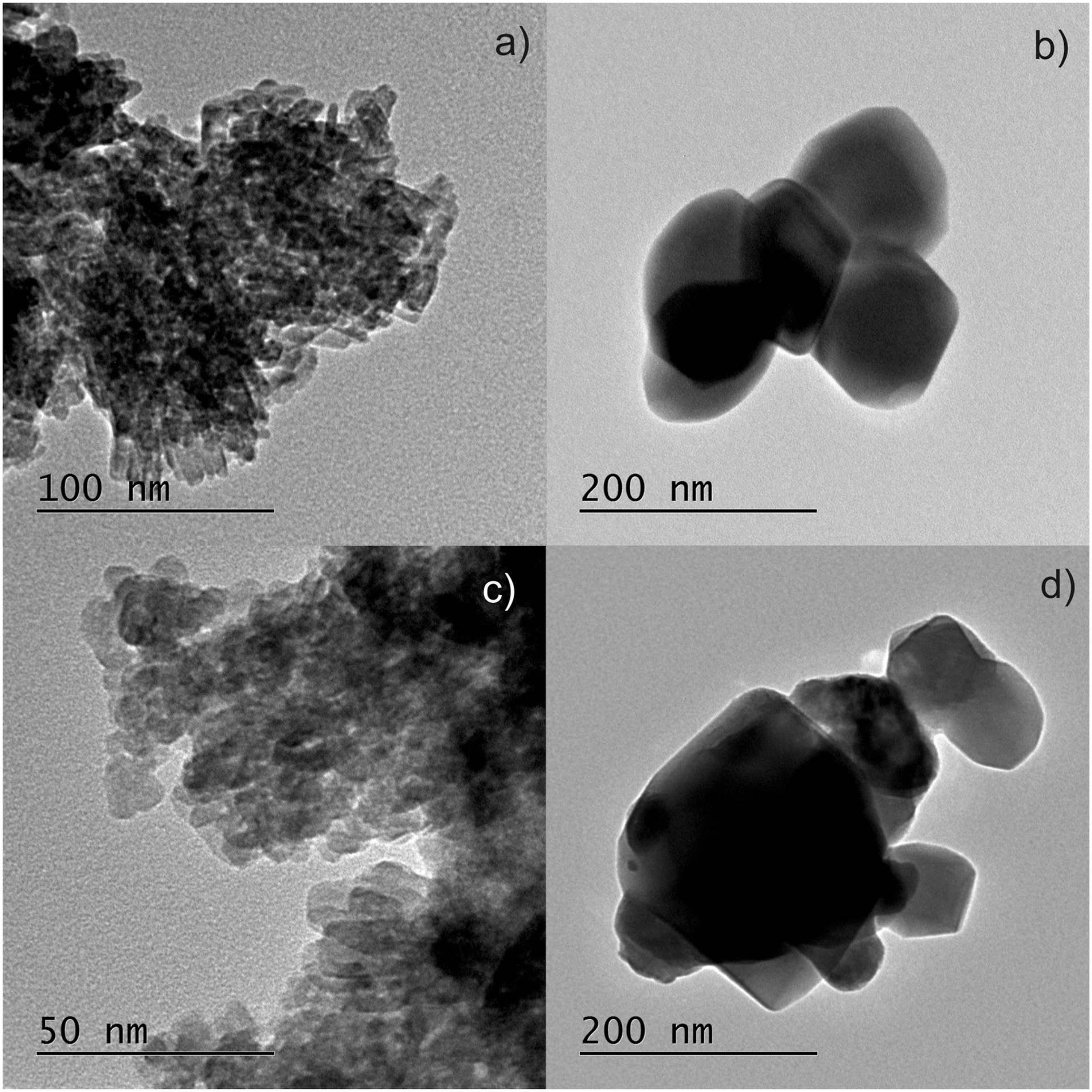
a)
100 nm
b)
200 nm
c)
50 nm
d)
200 nm

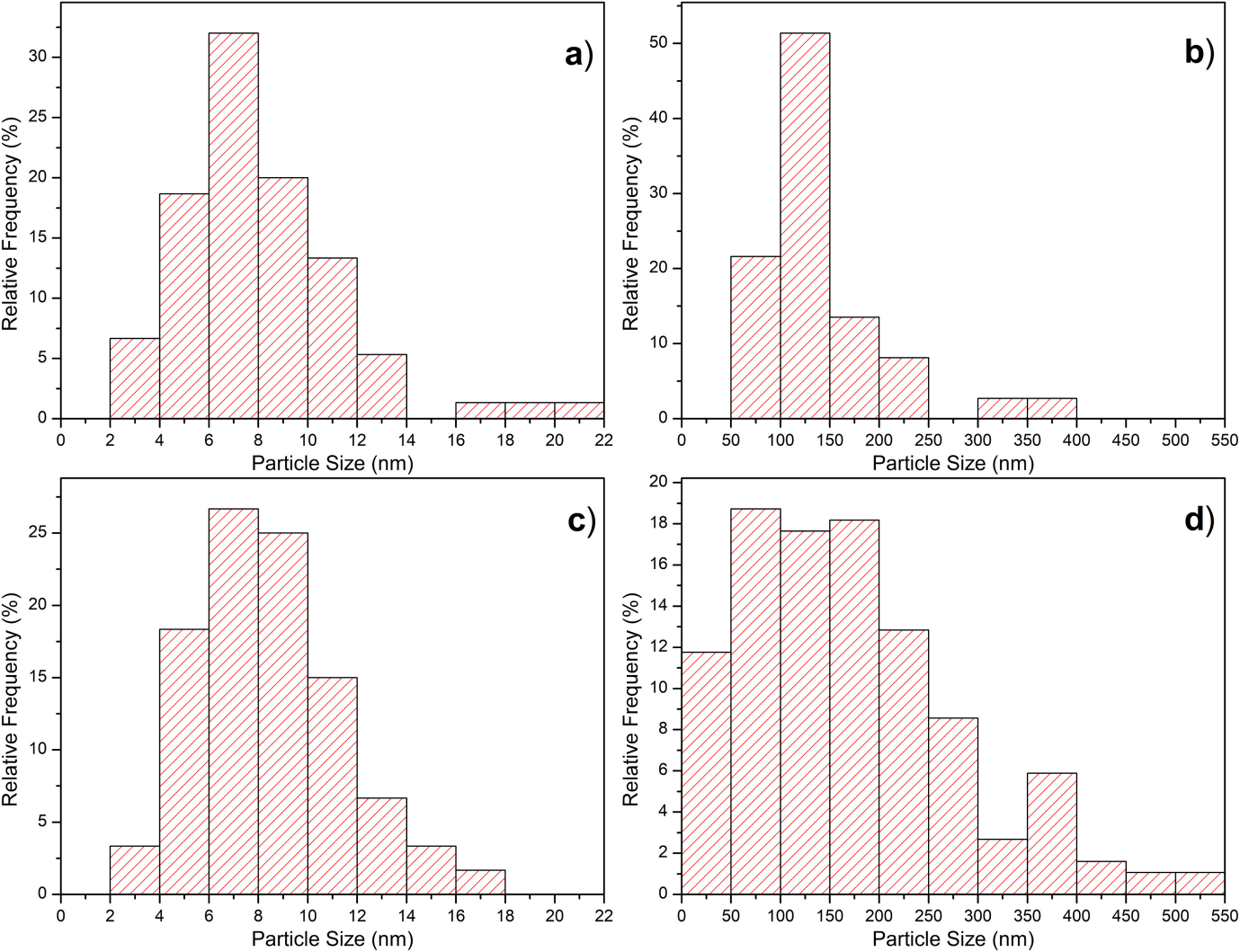
a)
Relative Frequency (%)
Particle Size (nm)
b)
Relative Frequency (%)
Particle Size (nm)
c)
Relative Frequency (%)
Particle Size (nm)
d)
Relative Frequency (%)
Particle Size (nm)

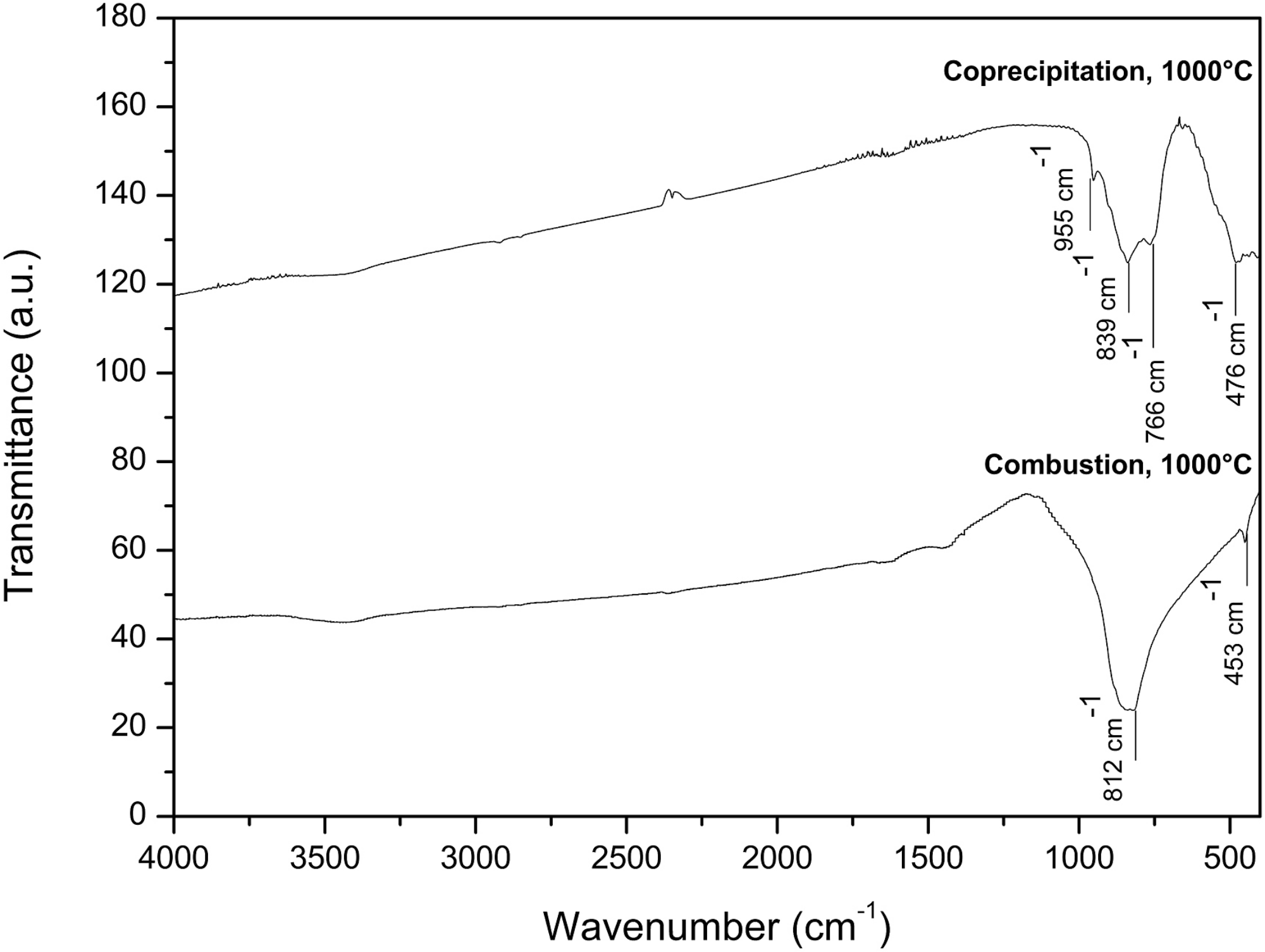
Coprecipitation, 1000°C
955 cm-1
839 cm-1
766 cm-1
476 cm-1
Combustion, 1000°C
812 cm-1
453 cm-1
Transmittance (a.u.)
Wavenumber (cm-1)
0
20
40
60
80
100
120
140
160
180
4000
3500
3000
2500
2000
1500
1000
500

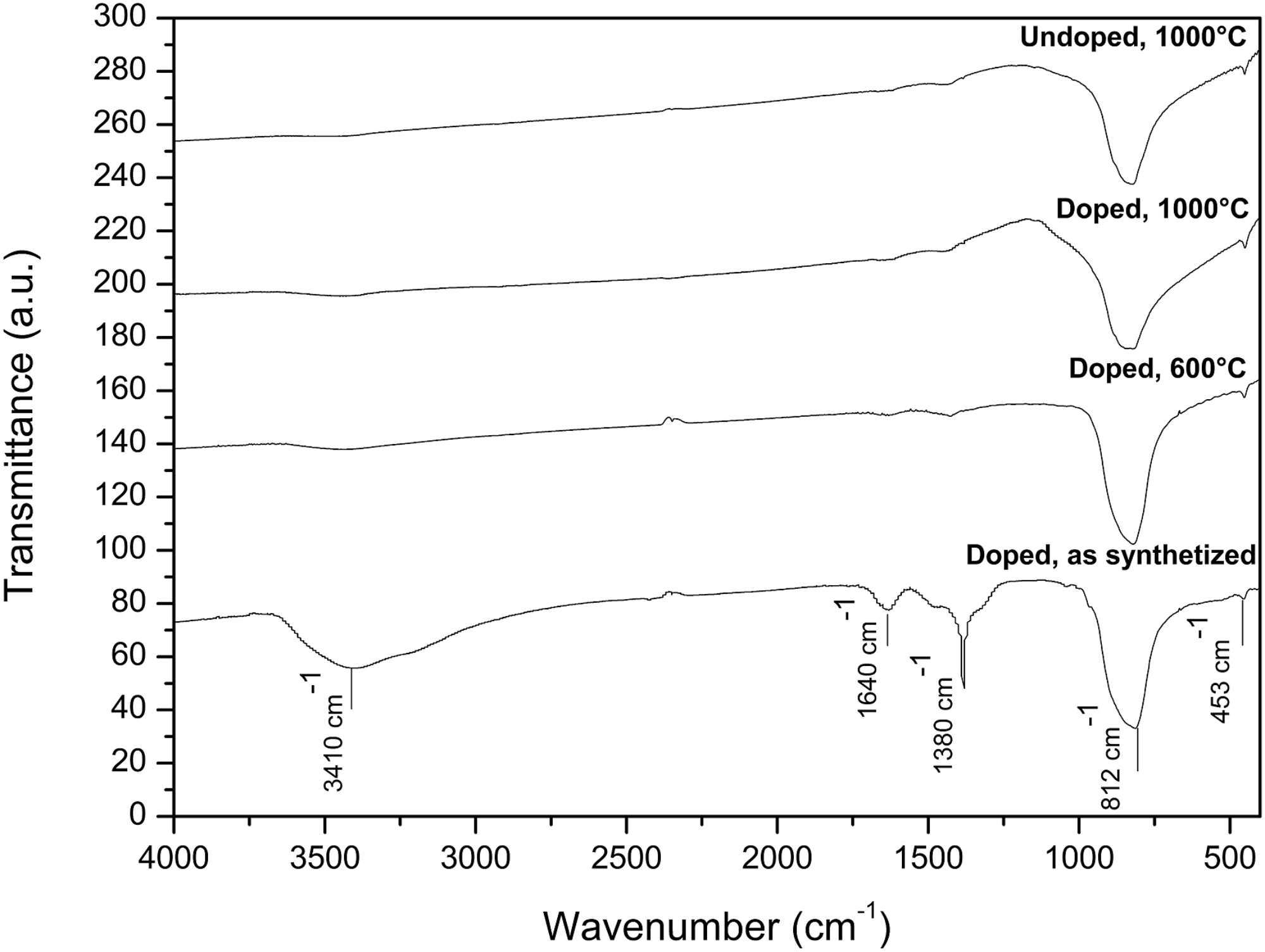
Undoped, 1000°C
Doped, 1000°C
Doped, 600°C
Doped, as synthetized
3410 cm-1
1640 cm-1
1380 cm-1
812 cm-1
453 cm-1
Transmittance (a.u.)
Wavenumber (cm-1)
0
20
40
60
80
100
120
140
160
180
200
220
240
260
280
300
4000
3500
3000
2500
2000
1500
1000
500

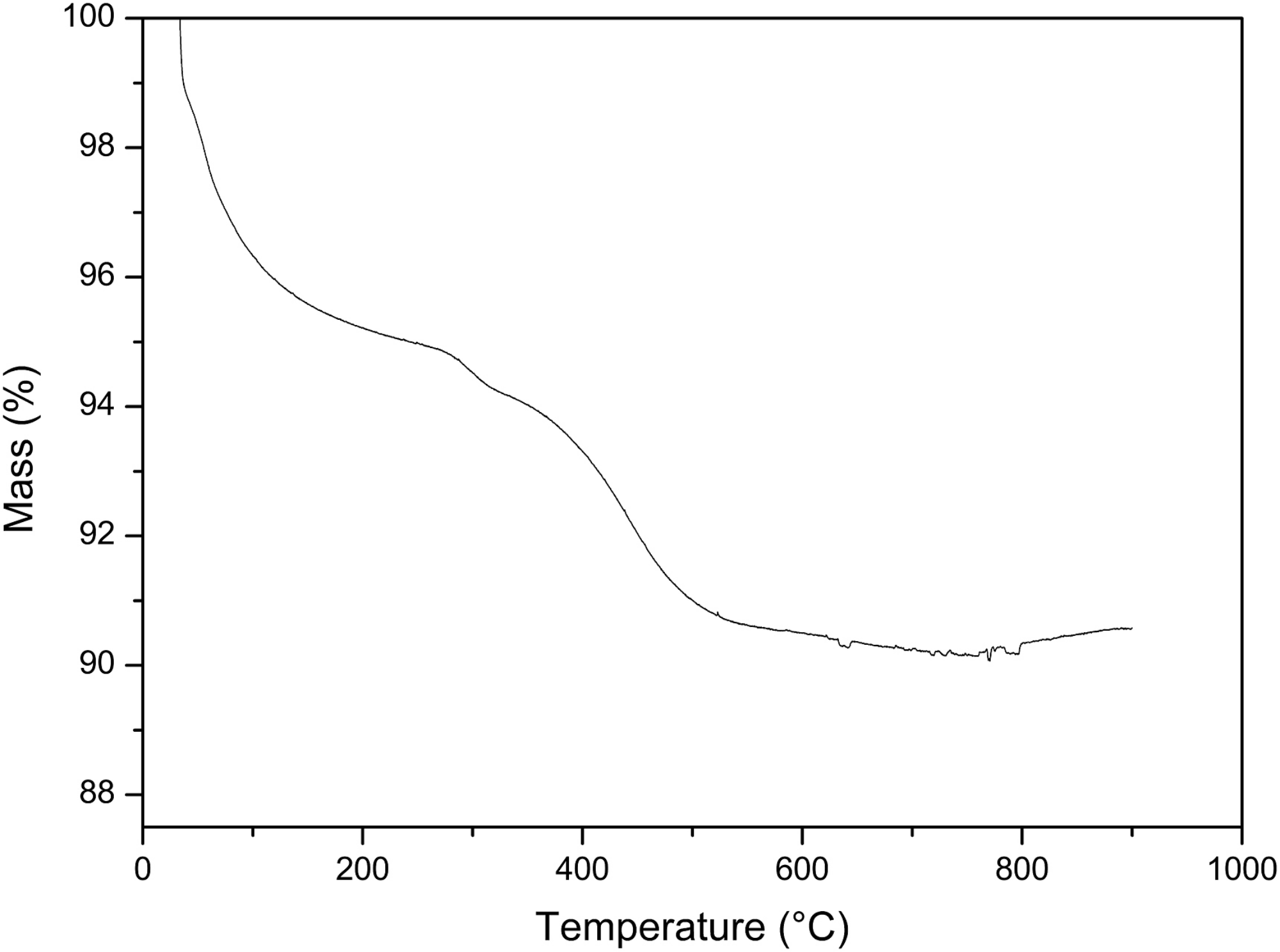
100
98
96
94
92
90
88
Mass (%)
0
200
400
600
800
1000
Temperature (°C)

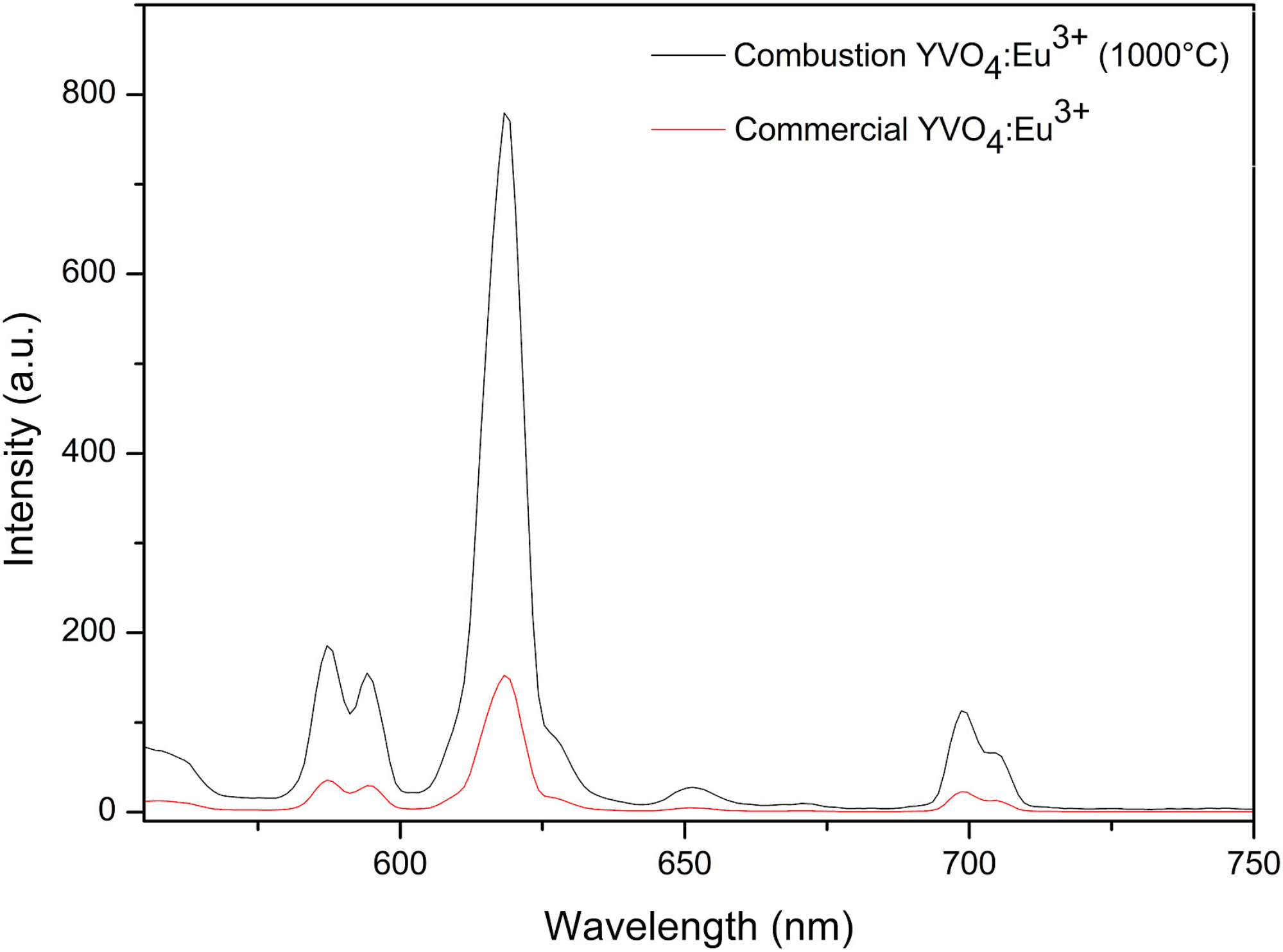
Combustion YVO4:Eu3+ (1000°C)
Commercial YVO4:Eu3+
Intensity (a.u.)
0
200
400
600
800
600
650
700
750
Wavelength (nm)

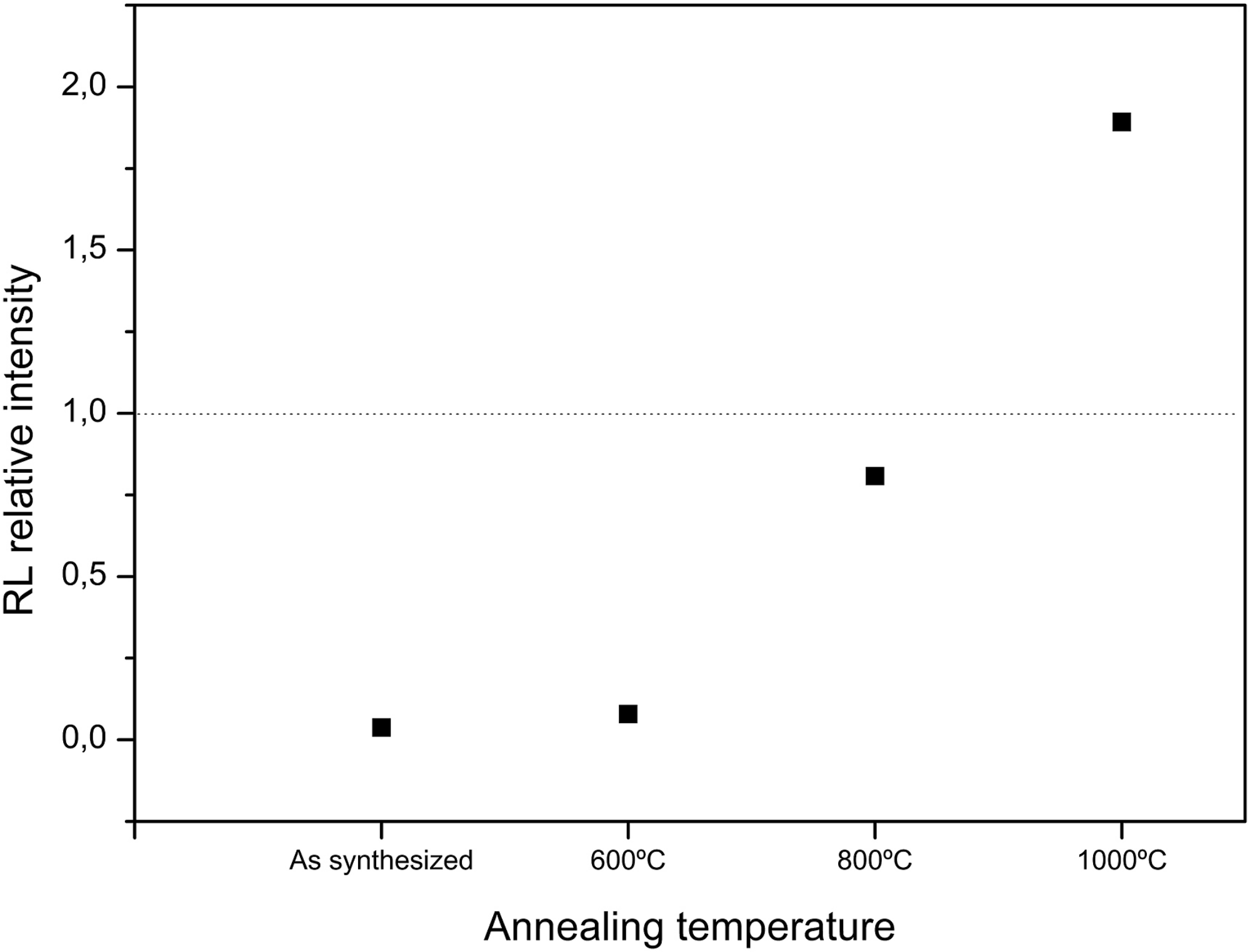
2,0
1,5
1,0
0,5
0,0
RL relative intensity
As synthesized
600ºC
800ºC
1000ºC
Annealing temperature

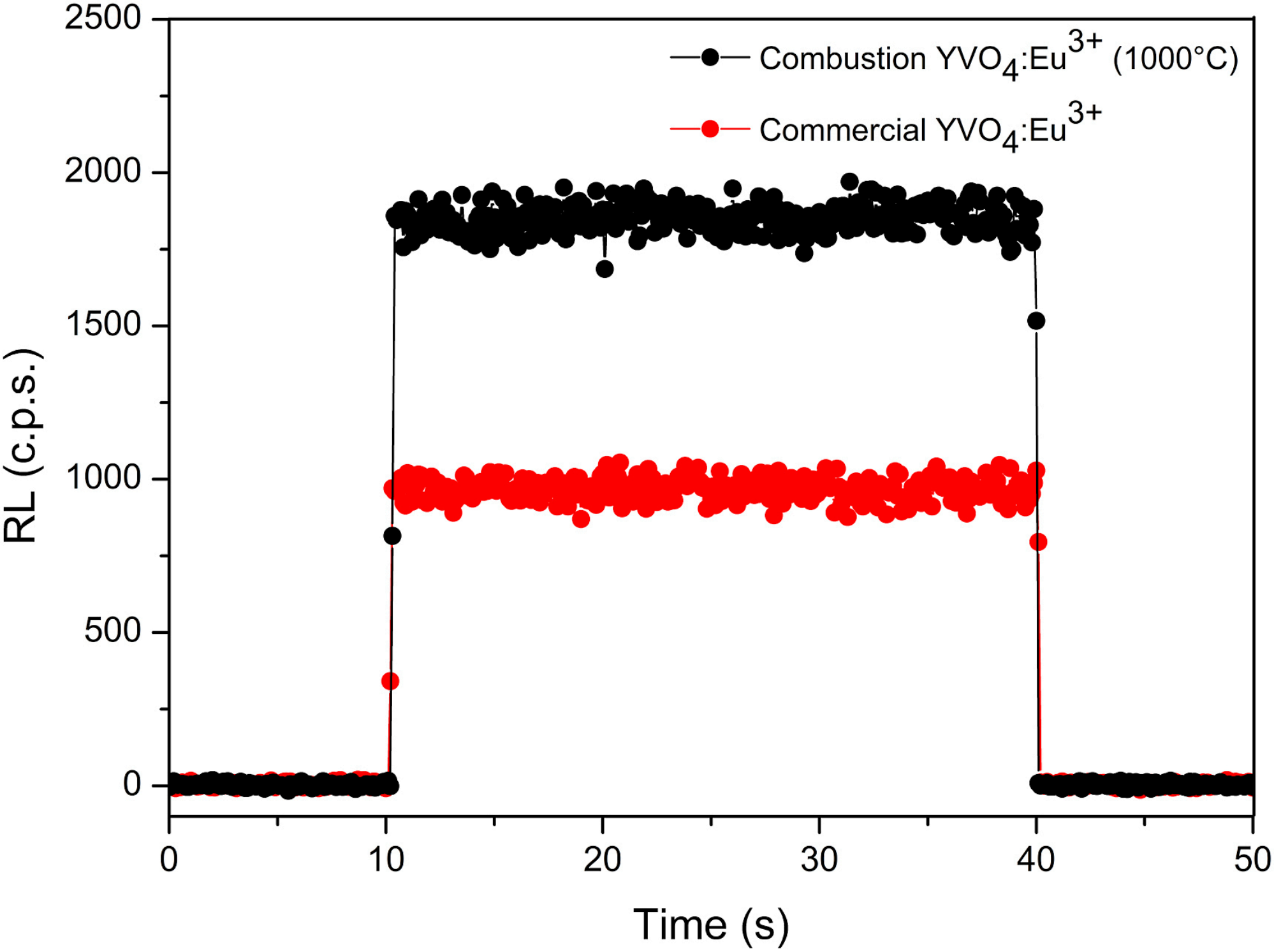
Combustion YVO4:Eu3+ (1000°C)
Commercial YVO4:Eu3+
RL (c.p.s.)
Time (s)
2500
2000
1500
1000
500
0
0
10
20
30
40
50

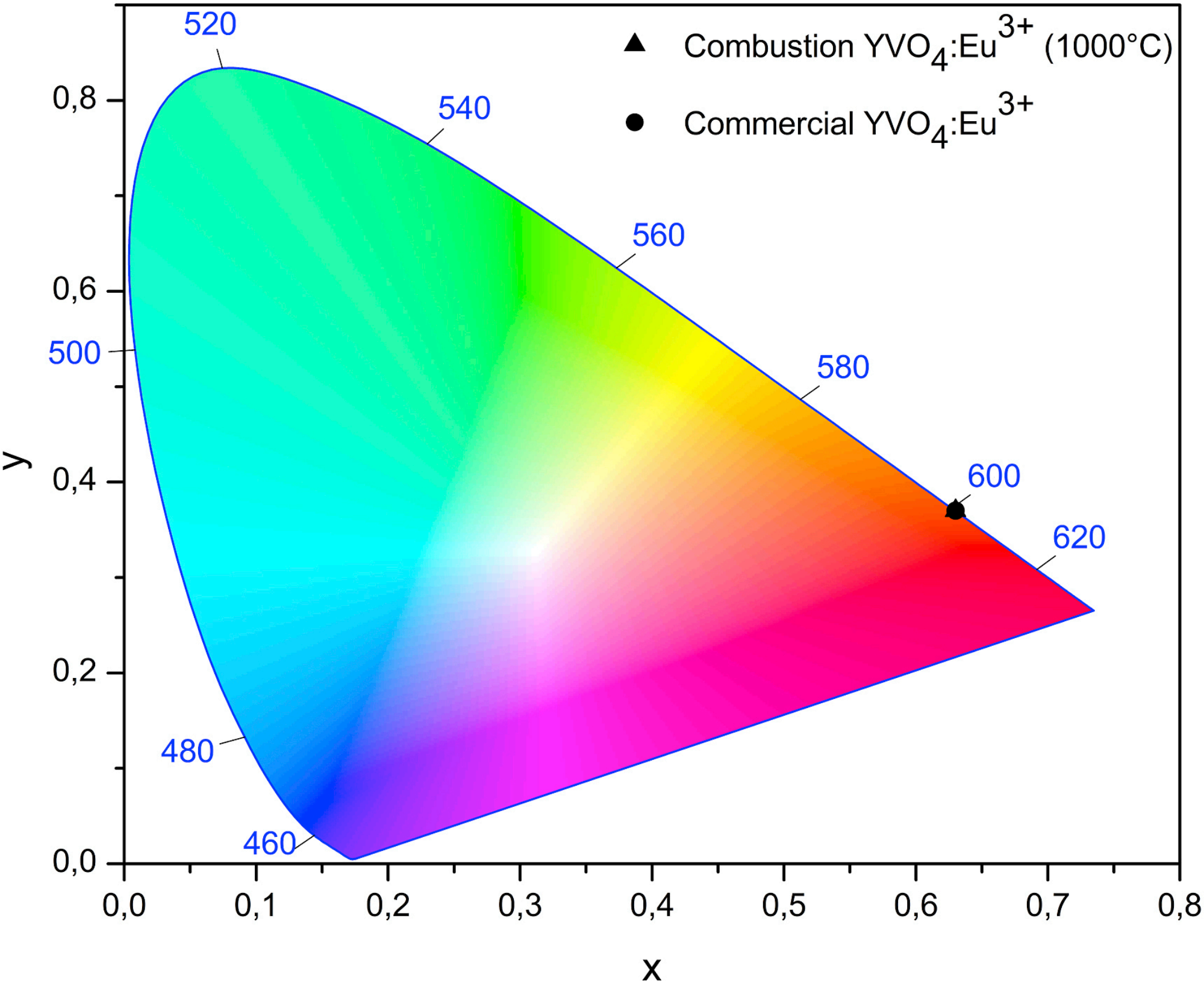
520
540
560
580
600
620
500
480
460
Combustion YVO4:Eu3+ (1000°C)
Commercial YVO4:Eu3+
0,0
0,2
0,4
0,6
0,8
y
0,0
0,1
0,2
0,3
0,4
0,5
0,6
0,7
0,8
x

Highlights

Combustion route is a simple synthesis method to obtain $YVO_4:Eu^{3+}$ nanoparticles.

Radioluminescence intensity is twice higher than that of microcrystalline sample.

$YVO_4:Eu^{3+}$ synthesized are suitable scintillators for Fiber Optic Dosimetry.

Declaration of interests

☒ The authors declare that they have no known competing financial interests or personal relationships that could have appeared to influence the work reported in this paper.

☐The authors declare the following financial interests/personal relationships which may be considered as potential competing interests: